PCCP

Accepted Manuscript

ROYAL SOCIETY OF CHEMISTRY

rsc.li/pccp

View Article Online
DOI: 10.1039/C7CP01333G

Journal Name

ARTICLE

Received 00th January 20xx,
Accepted 00th January 20xx

DOI: 10.1039/x0xx00000x

www.rsc.org/

Adapting BODIPYs to singlet oxygen production on silica nanoparticles

Nerea Epelde-Elezcano,[a] Ruth Prieto-Montero,[a] Virginia Martínez-Martínez,[a*] María J. Ortiz,[a] Alejandro Prieto-Castañeda,[b] Eduardo Peña-Cabrera,[c] José L. Belmonte-Vázquez,[c] Iñigo López-Arbeloa,[a] Ross Brown[d] and Sylvie Lacombe[d*]

A modified Stöber method is used to synthesize spherical core-shell silica nanoparticles (NPs) with an external surface functionalized by amino groups and with an average size around 50 nm. Fluorescent dyes and photosensitizers of singlet oxygen were fixed, either separately or conjointly, respectively in the core or in the shell. Rhodamines were encapsulated in the core with relatively high fluorescence quantum yields (Φ_{fl} ≥ 0.3), allowing fluorescence tracking of the particles. Various photosensitizers of singlet oxygen (PS) were covalenty coupled to the shell, allowing singlet oxygen production. The stability of NP suspensions strongly deteriorated upon grafting the PS, affecting their apparent singlet oxygen quantum yields. Agglomeration of NPs depends both on the type and on the amount of grafted photosensitizer. New, lab-made, halogenated 4,4-difluoro-4-bora-3a,4a-diaza-s-indacenes (BODIPY) grafted to the NPs achieved higher singlet oxygen quantum yields (Φ_{Δ} ~ 0.35-0.40) than Rose Bengal (RB) grafted NPs (Φ_{Δ} ~ 0.10-0.27). Finally, we combined both fluorescence and PS functions in the same NP, namely a rhodamine in the silica core and a BODIPY or RB grafted in the shell, achieving the performance Φ_{fl} ~ 0.10-0.20, Φ_{Δ} ~ 0.16-0.25 with a single excitation wavelength. Thus, proper choice of the dyes, of their concentrations inside and on the NPs and the grafting method enables fine-tuning of singlet oxygen production and fluorescence emission.

[a] Departamento de Química Física, Universidad del País Vasco-EHU. Apartado 644, 48080, Bilbao, Spain
[b] Departamento de Química Orgánica I, Facultad de Ciencias Químicas, Universidad Complutense de Madrid, Ciudad Universitaria s/n, 28040, Madrid, Spain.
[c] Chemistry Department, University of Guanajuato. Noria Alta S/N 36050. Mexico
[d] IPREM UMR CNRS 5254, Université de Pau et des Pays de l'Adour, Hélioparc, 2 av. Président Angot, 64053 Pau Cedex 09, France. [§]IPREM UMR CNRS 5254, Université de Pau et des Pays de l'Adour, Hélioparc, 2 av. Président Angot, 64053 Pau Cedex 09, France.
† Corresponding authors: sylvie.lacombe@univ-pau.fr; virginia.martinez@ehu.eus.
Electronic Supplementary Information (ESI) available: Experimental procedures, ^{1}H NMR and ^{13}C NMR spectra, DSL results, FTIR spectra, pictures of NP in powder and in suspension, photophysical data of fluorescent NPs, calculations of the number of dye molecules and their intermolecular distance in the silica nanoparticle.
See DOI: 10.1039/x0xx00000x

Introduction

Production of singlet oxygen ($O_2(a^1\Delta_g)$, $^1O_2$ in the following) through photosensitization involves three components: a photosensitizer (PS), a light source and oxygen. The development of photosensitizing *materials* is an active research field since singlet oxygen is very useful for numerous applications. Industrial uses include oxidation reactions of high added value under mild conditions such as oxidation of fine chemicals in organic solvents[1,2] and wastewater treatment.[3] Clinical uses include bactericidal or cancer treatments by applying photodynamic therapy.[4,5,6] In all applications, the photosensitizer has to be deposited, embedded or grafted on an inert substrate with suitable form, specific surface area and surface properties.[7] Such supported PSs have numerous advantages: improved recovery of unspent materials, control of aggregation and self-quenching of the PS, increase of PS photostability, possible use of solvents where the PS is poorly soluble or even use in solvent-free reactions.

Tailor-made nanoparticles (NP) used in the field of cancer therapy and diagnosis, are of current interest to enhance activity, delivery and targeting.[8,9] However several problems may arise such as the stability of the NP suspensions in various solvents due to aggregation or interaction between dyes in the same particle. Here, we focus on these aspects for silica NPs.

Indeed, among NPs, core-shell silica nanoparticles provide an opportunity to introduce different types of compounds with various properties, either grafted on the functionalized NP surface (shell) or embedded inside pores (core). Therefore, an increasing number of researchers have considered the use of silica nanoparticles for numerous medical applications[10–12]: platforms for PDT,[13–16] bioimaging probes,[17–19] combined uses such as theragnostics (therapy and diagnostics),[20–22] or drug delivery.[23,24] The main advantages of silica NPs are chemical inertness, transparency, porosity tuning insensitive to swelling or alterations with pH, good biocompatibility and easy functionalization of their surface.[25,26] A silica matrix thus provides a stable chemical and mechanical environment for an encapsulated fluorophore, protecting it from external perturbations,[27] which is of special interest in bioimaging where NPs can be monitored by optical techniques both in *vitro* and in *vivo*.[28] Conversely, the PS is better grafted on the outer surface to favour sensitization and delivery of singlet

View Article Online
DOI: 10.1039/C7CP01333G

oxygen. This implies that a functional group on the PS reacts with another functional group on the silica substrate. Among classical PSs, such as xanthene dyes, anthracene derivatives, porphyrins and phthalocyanins or aromatic ketones,[29,7] the carboxylate moiety of commercial Rose Bengal is easily coupled to various substrates.[30,31] Rose Bengal is a popular reference for singlet oxygen production in polar solvents such as in ACN or MeOH because of its high singlet oxygen quantum yield (Φ_Δ 0.5-0.8 in the visible region, λ_{abs} 550 nm). Its principal disadvantage is its susceptibility to photobleaching.

On the contrary, BODIPYs (base motif 4,4-difluoro-4-bora-3a,4a-diaza-s-indacene) are better known for their photostability and high extinction coefficients in the visible region than for the sensitization of singlet oxygen.[32,33] Here we exploit the versatility of BODIPY synthesis to produce a novel graftable sensitizer of singlet oxygen. Indeed, although BODIPY dyes usually exhibit negligible efficiency of triplet formation and high fluorescence quantum yields, the incorporation of heavy atoms (mainly iodine) directly to the BODIPY core enhances the spin–orbit coupling, thereby favouring intersystem crossing to the triplet state.[5,32,34,35,36,37] BODIPYs can also be modified to introduce grafting functionality to various solid substrates *via* carboxylate or amino groups.

In this work, we compare Rose Bengal and two new lab-made BODIPYs when grafted to core-shell silica NPs, particularly singlet oxygen quantum yields (Φ_Δ) and NP aggregation due to surface modification. The coupling process was first optimized with commercial Rose Bengal (RB1) and further applied to the BODIPYs (Figure 1) since to the best of our knowledge the grafting of BODIPYs on nanoparticles for singlet oxygen generation was up to now hardly investigated.[38,39] In a second step, we describe core-shell NPs with dual activity, combining both imaging, by embedding fluorescent rhodamines in the core, and singlet oxygen production, by grafting singlet oxygen photosensitizers in the shell. We also show the importance of controlling Förster resonance energy transfer (FRET) in such small particles. Combining two dyes in one particle can then achieve the contradictory aims of high fluorescence yield and high singlet oxygen sensitization with a single excitation wavelength.

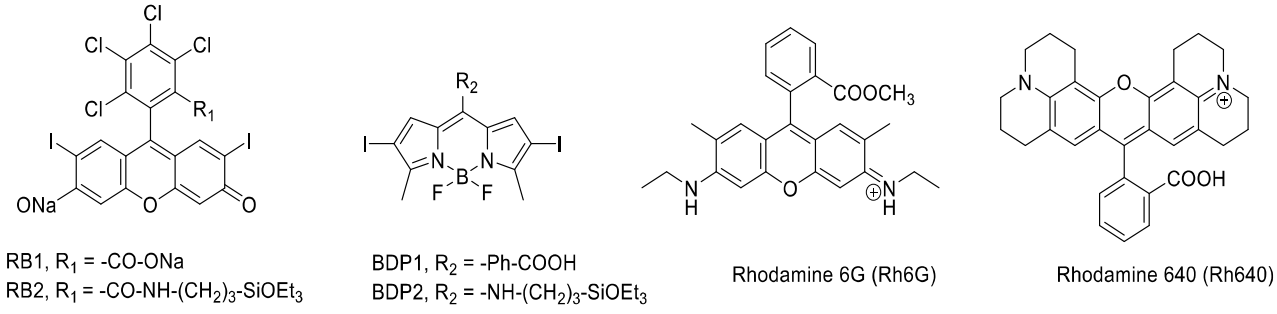

Figure 1. Structure of the used dyes

Results and discussion

In this work, mesoporous silica nanoparticles were prepared according to the Stöber methodology based on the sol-gel process with an additional reactant added to the system, namely a surfactant:[40,41] in the first step the core was synthesized through the mixture of an alkoxide in a water/alcohol solvent using ammonium hydroxide as a catalyst and CTAB (cetyl trimethylammonium bromide) surfactant. In a second step, addition of 3-aminopropyltrimethoxy-silane (APTMS) builds the shell containing amino groups for surface functionalization (Figure 2).

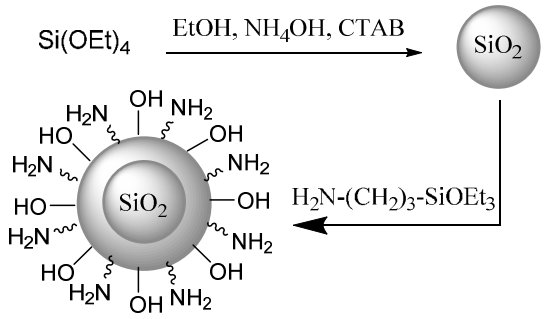

Figure 2. Synthesis of the core-shell silica nanoparticles by modification of the Stöber method.

For imaging applications, two highly fluorescent rhodamines (Rh6G, λ_{em} 530 nm and Rh640, λ_{em} 550 nm, Figure 1) were introduced in the initial alcohol solvent of the core xerogel. The PS grafting process at the surface (shell) was first optimized with Rose Bengal (RB1 and RB2) and implemented with alternative lab-made BODIPYs (BDP1 and BDP2) (Figure 1). Original synthesis schemes were used, based on the starting thioBODIPY, 3,5-dimethyl-8-methylthioBODIPY.[42] The synthesis of BDP1 with a carboxyphenyl group in *meso* position was achieved *via* Suzuki coupling of *p*-carboxyphenylboronic acid with thioBODIPY followed by iodination to yield the same compound as in [43]. BDP2 was prepared in two steps by iodination of the thioBODIPY, followed by nucleophilic substitution of the thiomethyl group with (3-aminopropyl)triethoxysilane. Two grafting methods were evaluated: either a peptide coupling reaction between surface-NH_2 of the silica shell and PS containing a carboxylic group such as RB1 or BDP1 (NP-RB1, NP-BDP1) or direct

View Article Online
DOI: 10.1039/C7CP01333G

polymerization of a PS containing a triethoxysilyl group (RB2 or BDP2) on the surface OH-group of silica (NP-RB2 or NP-BDP2) (Scheme S1, ESI).

3.1. Characterization and optimization of the silica nanoparticles

The composition of the NPs was derived from XPS results (Table 1). XPS data confirmed the major contribution of SiO_2 for NPs and the relative atomic ratio of N atoms around 4 % in the bare particles. The presence of the I and F atoms, as well as the higher contribution of the C and N atoms on both NP-BDP1 and NP-BDP2, are indicative of the successful grafting of BDP.

IR-ATR of the grafted NP-RB1, NP-RB2 and NP-BDP1 confirmed the presence of amide I (around 1630 cm^{-1}, C=O stretch) and amide II bonds (around 1550 cm^{-1}, C-N stretch and N-H bend) (Figure S2, ESI).[44] Conversely, this amide bond is not present in NP-BDP2 since they are obtained by direct polymerization of BDP2 on OH groups of the silica surface.

According to Table 1 (more details in Experimental Section), the amount of PS grafted on the silanol groups (NP-RB2 and NP-BDP2) is slightly higher than the PS grafted on the functional NH_2 groups (NP-RB1 and NP-BDP1). This reflects the higher amount of silanol groups compared to active NH_2 groups.

The nanoparticles had diameters around 50 nm, homogeneously distributed according to the SEM image (Figure 3 left) with a shell thickness around 10 nm (Figure 3 middle). The mesoporous structure of the silica NP is also nicely observed by TEM (Figure 3 right). TEM images also confirmed that the grafting process did not modify the spherical morphology and distribution, with particles size around 50 nm before and after grafting (Figure S3). Dynamic light scattering (DLS) measurements were performed to evaluate the NP size distribution, their dispersion and stability in different solvents with different polarity such as water, ethanol and acetonitrile (Table S1, Figure S1, ESI). The DLS measurements were done just after magnetic stirring of the NPs in a given solvent (t_0) and after one hour (t_1) without stirring.

Table 1. Spectrophotometric estimation of the amount of grafted PS on silica NPs (suspensions in $CHCl_3$) and % atomic concentration on their surface from XPS results.

Sample	PS amount (μmol gr^{-1})		% At Concentration						
			C	O	N	Si	Cl*	F	I
NP	Meth.1‡	Meth.2‡	15	52	4.0	26	2.5	-	-
NP-BDP1	-	1.8	22	44	7	22		2.3	2.2
NP-BDP2	-	5.2	23	42	5.1	24	2.4	2.2	1.6
NP-RB1	8.0	-	-	-	-	-	-	-	-
NP-RB2	24	-	-	-	-	-	-	-	-

‡ More details about method 1 and method 2 in Experimental Section.

* The presence of chlorine atoms in bare NP and NP-BDP2 (2.5 % atomic ratio) is due to the washing of the nanoparticles by a diluted hydrochloric solution at the end of the synthesis, transforming the amino groups into ammonium chloride groups. For NP-RB1 and NP-BDP1, chlorine atoms were removed by addition of triethylamine.

All samples analyzed at t_0 showed only one distribution curve with similar hydrodynamic diameters (212±13 nm and 257±54 nm in ethanol and water respectively, indicating agglomeration of the NPs in these solvents. However, in ACN, the NP size distribution was considerably lower showing a better dispersion of NPs (92±3 nm). Nevertheless, important changes in the hydrodynamic diameter occurred after 1 hour without stirring; in ethanol higher aggregates were formed, while in water and ACN two different NP populations were obtained with larger aggregates together with better dispersed NPs (Table S1 and Figure S1, ESI). According to the DLS experiments, ACN was an appropriate solvent for the bare silica nanoparticles. The DLS results for the different grafted-NP in ACN and in $CHCl_3$ just after magnetic stirring (t_0) are included in Table S2. After the grafting process, depending both on the type of photosensitizer and on the grafting method, the stability of the suspension is greatly modified, as shown by the increase of the hydrodynamic diameter in ACN, in the order bare NP< NP-BDP1<NP-BDP2<NP-RB1. Generally speaking, BDP-grafted NPs are more stable in suspensions compared to RB-grafted NPs.

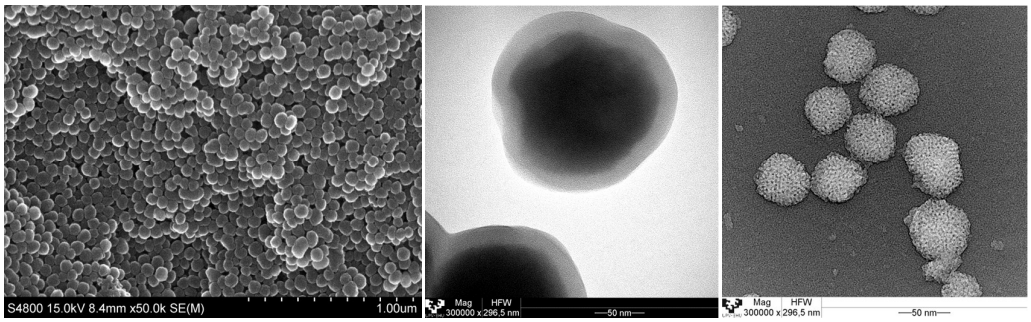

Figure 3. (Left) SEM images of silica NPs with around 50 nm size; (Middle) TEM image of the Core-Shell Silica NP and (Right) TEM image of the mesoporous structure of the silica NPs.

View Article Online
DOI: 10.1039/C7CP01333G

Journal Name

ARTICLE

3.2. Photophysical properties and singlet oxygen production by PS grafted on NPs

Contrary to bare NPs, no suitable solvent was found to obtain stable nanoparticle suspension for NP-RB2, while in the less polar chloroform, NP-RB1 suspension was more stable (Figure S3, ESI).[45] We refer here to resistance against precipitation not photostability. On the contrary, stable suspensions of NP-BDP1 and NP-BDP2 were obtained in both acetonitrile and chloroform. Contrary to bare NPs, fast precipitation of both NPs was observed in water. These data suggest significant surface modification on NP-RB samples, while surface modification was much less significant on NP-BDP.

All the absorption bands of NP-grafted PSs are slightly broader than in solution (Figure 4).[44,46] The absorption spectra of NP-RB1 and NP–RB2 show a main band centred at 561 nm with a shoulder around 514 nm, more prominent than in solution (Figure 4 A and B). On the other hand, the absorption spectra of NP-BDP1 and NP-BDP2 show no significant modification in any solvents (Figure 4 C and D).

At first sight, these observations are consistent with the well-known tendency of xanthene dyes (RB) to aggregate in concentrated or rigid media. Indeed this kind of spectral deformation is often interpreted as an indication of *e.g.* H-aggregation.[29,44,47,48] Indeed, assuming purely random local fluctuations of the inter-dye molecule distances, from point to point on a NP, the classical Hertz distribution law in two dimensions implies significant fractions of paired molecules (see detailed calculations in ESI, §S4, Eqs S1-S5). However one must beware of artefacts in optically thick samples. This type of spectral shape, where a "new" shoulder is observed close in wavelength to an existing weak vibronic band is discussed in detail in [49] and references therein. The observed spectral changes could be due to the influence of multiple scattering in the sample. The fact that these scattering effects are much less severe in NP-BDP samples is in agreement with their already mentioned more stable suspensions (Table S2, Figure S4) and suggests that dye-mediated NP surface modification controls particle aggregation, hence scattering and the effective optical path length and finally the shape of the spectra. Unfortunately the small amounts of available NPs precluded further investigating these effects.

Note here that in the case of NP-RB, the dye-mediated agglomeration of NPs not only modifies the absorption spectra but also explains the reduced singlet oxygen generation (Table 2). Nonetheless, a higher singlet oxygen quantum yield was obtained with NP-RB1 in $CHCl_3$ suspension (Φ_Δ= 0.27, Figure S5) relative to ACN (Φ_Δ= 0.14, Figure S5), likely as a consequence of the better stability of the chloroform suspension compared to NP-RB2 (singlet oxygen values lower than 0.10). These results emphasize the importance of controlling the agglomeration of the NP-grafted photosensitizers. It is thus of crucial importance to obtain stable nanoparticle suspensions to obtain good singlet oxygen production for future implementation.

Figure 4. (A) Absorption spectra in ACN of NP-RB1 (red) and NP-RB2 (green) and of RB in diluted solution (black), (B) Absorption spectra in $CHCl_3$ of NP-RB1 (red) and NP-RB2 (green) (the spectra of RB in ACN solution (black) is also inserted for comparison), (C) Absorption spectra of BDP1 solution in ACN (black), NP-BDP1 suspension in ACN (red), NP-BDP1 suspension in $CHCl_3$ (green); (D) Absorption spectra of NP-BDP2 in ACN (red), in $CHCl_3$ (green) and of BDP2 in THF solution (black).

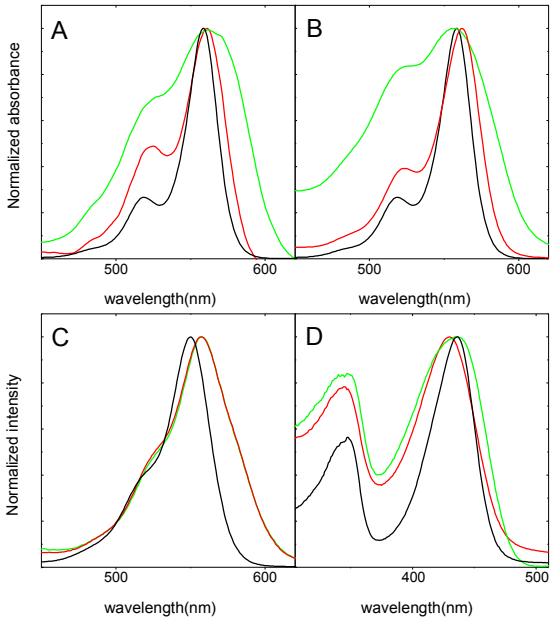

For the same reason, higher singlet oxygen quantum yields were obtained with NP-BDP, which remain stable in ACN and $CHCl_3$ suspensions (0.33 and 0.37 for NP-BDP1, 0.36 and 0.38 for NP-BDP2, respectively, Figure S5). These results are in agreement with the absorption spectra, indicating that both NP-BDPs are much less agglomerated. Thus, by using these BODIPYs as grafted PS, the range of solvent polarities suitable for stable NP suspensions is wider than with RB, leading to higher singlet oxygen quantum yields (although lower than with the corresponding BDP in solution, Table 2).[35] These results are in agreement with previous data on singlet oxygen detection with NPs containing a covalently encapsulated

View Article Online
DOI: 10.1039/C7CP01333G

BODIPY similar to BDP1 (with four methyl groups on the indacene core) in toluene suspension. However no singlet oxygen quantum yield was measured in this earlier study.[50] Triplet quantum yields would in general be a very useful complement to the singlet quantum yields but was not achievable within the scope of this paper or, apparently, in the literature on this kind of systems. It is to be hoped that future work in this field will address this point. [35,38,50]

Table 2. Photophysical data and quantum yield of singlet oxygen production of grafted nanoparticles compared with the corresponding dyes in ACN or $CHCl_3$ solutions and of dual NP/R640-BDP1 and NP/R6G-RB1 suspended in $CHCl_3$.

	λ_{abs} (nm)	λ_{fl} (nm)	Φ_{fl}	Φ_Δ	
				ACN	CHCl3
RB1	555	579	0.12	0.52[1]	-
NP-RB1	561	580	0.08	0.14[2]	0.27[3]
NP-RB2	561	584	0.03	0.10[2]	0.07[3]
BDP1	550	578	0.03	0.66[2]	-
NP-BDP1	560	580	≤0.01	0.33[2]	0.37[3]
BDP2	426	484	0.02	0.78[1]	-
NP-BDP2	430	494	≤0.01	0.36[1]	0.38[3]
NP-Rh640	568	590	0.56	-	-
NP-Rh6G	530	550	0.30	-	-
NP/Rh640-BDP1	564	583	0.10	-	0.16[3]
NP/Rh6G-RB1	561	580	0.20	-	0.25[3]

[1]measured in our laboratory by direct method with phenalenone as reference (Φ_Δ = 1 in ACN) [51]
[2]Reference RB in ACN (Φ_Δ=0.52)
[3]Reference 8-methylthio-2,6-diiodoBODIPY, 2I-ThioBDP in $CHCl_3$ (Φ_Δ = 0.85).[35]

3.3. NPs with dual functionality

With a view to tracing the particles (environmental tracing, recovery or bio-imaging), a fluorescent dye (Rh6G or Rh640) was embedded in the silica nanoparticle. In order to optimize the fluorescent properties of the rhodamine core, different concentrations of Rh6G in the alcohol of the sol-gel synthesis were checked in the range of 10^{-2} - 5.0 x 10^{-5} M. The dye encapsulation did not modify the NP size, morphology and polydispersity (Figure S6, ESI). According to the photophysical properties of the fluorescent nanoparticles thus obtained (Table S3, Figure S7 and Figure S8 in ESI), the optimum concentration of rhodamines in the gel was about 5 x 10^{-4} M, achieving a dye loading in the core around 1 µmol g^{-1} (Table S3). As already reported, the fluorescence emission was higher at low dye loading.[22,52] More importantly, the fluorescence quantum yields of the powders (Φ_{flu} = 0.30 and 0.52 for Rh6G-NP and Rh640-NP, respectively), although lower than that of the dyes in solution (Table S3 in ESI), are high enough for detection under conventional fluorescence microscopes and therefore adequate for bio-imaging (Figure S7 D and E).

Two different strategies were designed to combine the fluorescent dye with the photosensitizer in the same NP: *i*) different absorbance range (NP noted NP/Rh640-BDP2) in order to selectively activate the different actions (fluorescence under green excitation and singlet oxygen production under blue light) by using different wavelengths; *ii*) similar absorption range for both dyes (NP noted NP/Rh6G-RB1 and NP/Rh640-BDP1) in order to use only one excitation light to trigger both functions (Figure 5).

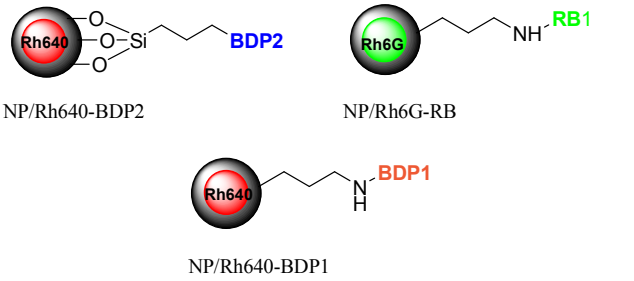

Figure 5. Scheme of the various NPs with dual functionalities.

The absorption spectra of NP/Rh640-BDP2 in chloroform suspension (Figure 6) show the characteristic bands of both dyes at 438 nm (BDP2) and 572 nm (Rh640). The BDP2 absorption band is around 10 times more intense than that of Rh640, indicating a higher amount of the photosensitizer on the surface with respect to the fluorescent dye in the core, in agreement with the estimated concentration for each dye (5.2 and 0.67 µmol g^{-1}, Table 1 and Table S3). The emission band of Rh640 at 590 nm is also observed upon direct excitation of BDP2 (λ_{ex} = 440 nm) where the absorbance of the Rh640 is practically negligible. In line with this observation, the contribution of the BDP2 chromophore is also clearly seen in the excitation spectrum of NP/Rh640-BDP2, at the emission wavelength of Rh640 (575 nm) (Figure 6C). Moreover, the fluorescence decay of BDP2 is faster in presence of Rh640 (Figure 6D). All these data confirm that the excited state of Rh640 is populated by a Förster Resonance Energy Transfer process (FRET) from BDP2 to Rh640. The FRET is a consequence of the overlapping between the fluorescence band of BDP2 (donor) and the absorption band of Rh640 (acceptor) and its efficiency depends on the distance between them, which is typically in the range of 1-10 nm.[53] Indeed, the thickness of the shell, around 10 nm, allows FRET process from the BDP2 at the external surface to the fluorescent dye in the core of the silica nanoparticles. However, the FRET induces a negative consequence in the singlet oxygen quantum yield of NP/Rh640-BDP2: it is practically negligible due to a reduced intersystem crossing process from the singlet excited state of BDP2 to its triplet state in favour of energy transfer process from the singlet excited state of BDP2 to the singlet excited state of R640.

However, when combining the photosensitizer and the fluorescent dye with similar adsorption range in NP/Rh640-

View Article Online
DOI: 10.1039/C7CP01333G

BDP1 and NP/Rh6G-RB1, individual contributions in the absorption spectra are poorly distinguished. In the case of NP/Rh640-BDP1, the maximum absorption falls between those of both dyes (Figure 7 and Table S2), indicative of the presence of both chromophores, Rh640 (1.0 μmol g^{-1}) and BDP1 (1.8 μmol g^{-1}). On the other hand, for NP/Rh6G-RB1, the contribution of Rh6G appears in the stronger shoulder at 520 nm compared to NP/RB1 (Figure 7B). The estimated amont of Rh6G (0.67 μmol g^{-1}, Table S2) is about 5 times less than RB1 (3.3 μmol g^{-1}, Table 1) grafted on the external surface.

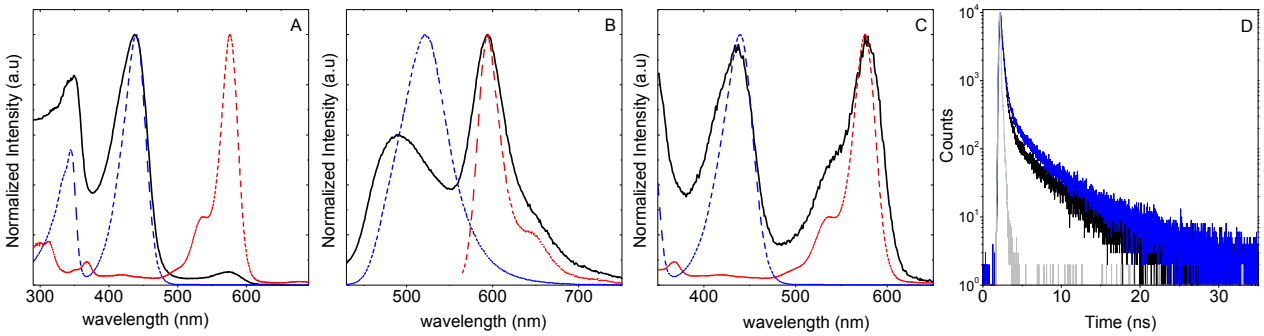

Figure 6. (A) Absorption spectra and (B) fluorescence spectra of NP/Rh640-BDP2 with λ_{ex} 440 nm (black) in $CHCl_3$. BDP2 (blue dotted lines) and Rh640 (red dotted lines) in a EtOH are inserted; (C) excitation spectra of NP/Rh640-BDP2 suspension in $CHCl_3$ at λ_{em} 575 nm (black), and the absorption spectra of BDP2 in ACN solution (blue dotted line) and Rh640 in EtOH solution (red dotted line). D) Fluorescence decay curves of NP/BDP2 (blue) and NP/Rh640-BDP2 (black) upon 400nm and 490 nm emission wavelength.

Importantly, NP/Rh640-BDP1 and NP/Rh6G-RB1 achieve a balance between the singlet oxygen quantum yield and the fluorescence quantum yields (Table 2). Particularly, NP/Rh640-BDP1 has a fluorescence quantum yield around 0.10 (Φ_{fl} = 0.56 for NP-Rh640) together with a singlet oxygen quantum yield of 0.16 (Φ_{Δ} = 0.37 for NP-BDP1). Even better, NP/Rh6G-RB1 has a fluorescence quantum yield around 0.20 (Φ_{fl} = 0.30 for NP-Rh6G) with a relatively high singlet oxygen quantum yield of 0.25 (Φ_{Δ} = 0.27 for NP-RB1).

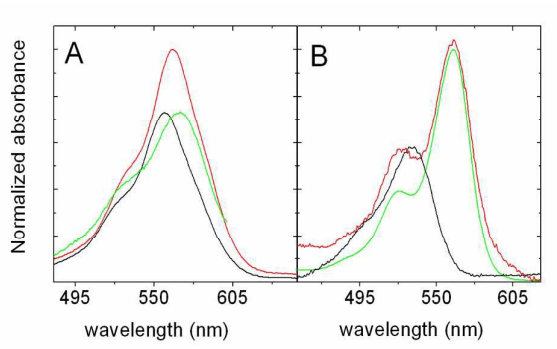

Figure 7. (A) Absorption spectra in $CHCl_3$ of; (A) NP/Rh640-BDP1 (red), NP-BDP1 (black) and NP-Rh640 (green), and **(B)** NP/Rh6G-RB1 (red), NP-Rh6G (black) and NP-RB1 (green).

Therefore, the combination of two dyes with complementary actions (high fluorescence *vs* high singlet oxygen production) but with overlapping absorption bands produced samples with dual functionality, which could be interesting for bio-imaging and PDT. Other combinations of chromophores can be combined with the aim of optimizing the dual action of NPs. The difficulty is reconciling the dual activity with the constraints of energy transfer. Earlier solutions to this problem required two excitation wavelengths. Zhang *et al.* designed dual core-shell nanoparticles embedding a fluorescent dye in the core (fluorescein isothiocynate, FITC) and a PS (hematoporphyrin, HP) in the shell.[54] In their case, the dual functionality in water suspensions was obtained using different triggering excitation light: 488 nm for fluorescence emission and 633 nm for singlet oxygen production. Estevao *et al.*, obtained dual functionality in aqueous suspensions of core-shell nanoparticles containing fluorescent rhodamine B in the core and verteporphin in the shell as PS for singlet oxygen production, triggered by two distinct excitation wavelength (520 and 690 nm respectively).[22]

Experimental

2.1. Synthesis of BDPs

Materials and methods

All starting materials and reagents were commercially obtained, unless indicated otherwise, and used without further purifications. Common solvents were dried and distilled by standard procedures. Flash chromatography was performed using silica gel (230-400 mesh). NMR spectra were recorded at 20 ºC in $CDCl_3$. ^1H chemical shifts are dated in ppm relative to tetramethylsilane (δ = 0.00 ppm) as internal standards. ^{13}C chemical shifts are dated in ppm with $CDCl_3$ (δ = 77.03 ppm) as the internal standard. DEPT 135 experiment was used to assign the type of carbon nucleus (C vs CH vs CH_2 vs CH_3). FTIR spectra were obtained from neat samples using the ATR technique. High-resolution mass spectrometry (HRMS) was performed using the EI technique. All the chemicals were purchased from Sigma-Aldrich, except BDP1 and BDP2 whose synthesis is show in Scheme 1. Detailed experimental procedures are given below. See the Supporting Information for the NMR spectra.

View Article Online
DOI: 10.1039/C7CP01333G

Synthesis of BDP1

Synthesis of BDP-COOH. Schlenk tube equipped with a stir bar was loaded with 3,5-dimethyl-8-methylthioBODIPY (100.0 mg, 0.38 mmol, 1.0 equiv.), *p*-carboxyphenylboronic acid (187.1 mg, 1.13 mmol, 3.0 equiv.), $Pd_2(dba)_3$ (8,6 mg, 0.009 mmol, 2.5 mol%), tri-2-furylphophine (6.5 mg, 0.028 mmol, 7.5 mol%), CuTc (214.2 mg, 1.13 mmol, 3.0 equiv.) and dry THF (0.03 M). The mixture was bubbled with N_2 for 5 min. The Schlenk tube was then immersed in a preheated oil bath at 55 ºC. The oil bath was removed after the starting material was consumed (90 min). After the mixture reached room temperature, the crude material was absorbed in silica gel, the solvent evaporated in vacuo, and the product was purified by flash chromatography using 20% EtOAc/hexanes as eluent. The desired product was obtained as a dark red solid (77.6 mg, 0.228 mmol, 61%). ^{1}H NMR (500 MHz, $CDCl_3$) δ 8.22 (d, *J* = 7.5 Hz, 2H), 7.61 (d, *J* = 7.6 Hz, 2H), 6.66 (s, 2H), 6.24 (d, *J* = 3.4 Hz, 2H), 2.66 (s, 6H) ppm.[43]

Synthesis of BDP1. To a solution of 8-*p*-carboxyphenyl-3,5-dimethylBODIPY (BDP-COOH) (45.4 mg, 0.13 mmol, 1.0 equiv.) in acetic acid (6 mL) was added dropwise a solution of *N*-chlorosuccinimide (48.0 mg, 0.36 mmol, 3.0 equiv) and NaI (54 mg, 0.36 mmol, 3.0 equiv.) in 4 mL of acetic acid. The reaction mixture was stirred at room temperature and monitored by TLC (EtOAc:hexane:acetic acid (15:84.5:0.5)). The reaction was stirred for 45 minutes. The crude material was neutralized with a saturated solution of $NaHCO_3$ in water and the product was extracted with CH_2Cl_2 (2 x 50 mL) and washed with water (2 x 25 mL). The combined organic layers were washed with brine (2 x 100 mL), dried over $MgSO_4$, filtered, and the volatiles were removed in vacuo and the product was purified by flash chromatography on silica gel using EtOAc/hexanes/acetic acid (30:69:1) as eluent. The desired product was obtained as a red waxy solid (0.02 mg, 0.034 mmol, 25%). ^{1}H NMR (500 MHz, DMSO-d_6) δ 8.09 (d, *J* = 7.4 Hz, 2H), 7.70 (d, *J* = 8.2 Hz, 2H), 7.09 (s, 2H), 2.56 (s, 6H) ppm.[30]

Synthesis of BDP2:

Synthesis of 2,6-diiodo-3,5-dimethyl-8-methylthioBODIPY (2I-ThioBDP). To a solution of 3,5-dimethyl-8-methylthioBODIPY[42] (32.0 mg, 0.12 mmol, 1.0 equiv.) in acetic acid (2 mL) was added dropwise a solution of *N*-chlorosuccinimide (48.0 mg, 0.36 mmol, 3.0 equiv) and NaI (54 mg, 0.36 mmol, 3.0 equiv.) in 2 mL of acetic acid. The reaction mixture was stirred at room temperature and monitored by TLC (EtOAc:hexane: (15:85)). The reaction was stirred for 30 minutes. The crude material was neutralized with a saturated solution of $NaHCO_3$ in water and the product was extracted with ethyl ether (3 x 15 mL) and washed with water (4 x 10 mL). The combined organic layers were washed with brine (2 x 50 mL), dried over $MgSO_4$, filtered, and the volatiles were removed in vacuo and the product was purified by flash chromatography on silica gel using EtOAc/hexane (2:8) as eluent. The desired product was obtained as green crystals (58.6 mg, 0.113 mmol, 94%). ^{1}H NMR (300 MHz, $CDCl_3$) δ 7.50 (s, 2H), 2.76 (s, 3H), 2.61 (s, 6H) ppm.).[55]

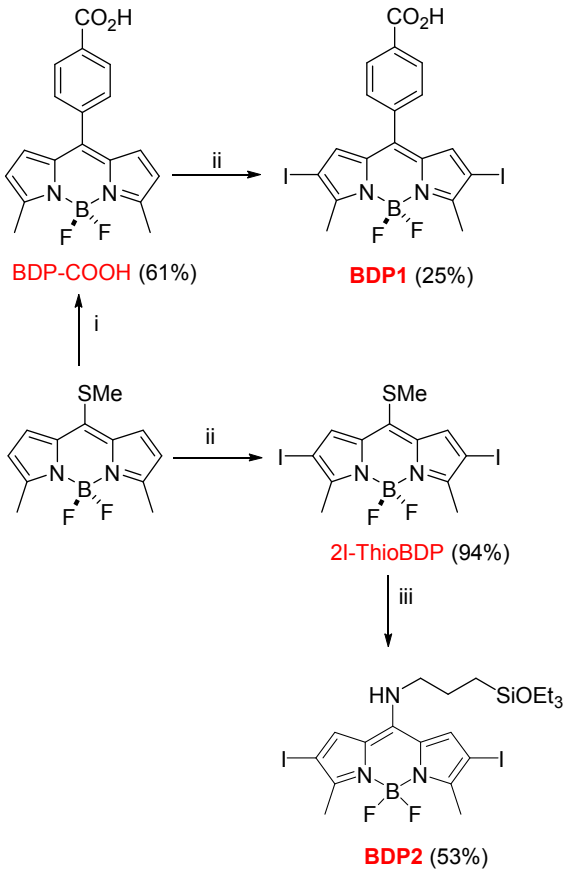

Conditions Reaction: i) *p*-CO_2H-C_6H_4-$B(OH)_2$, CuTC, 2.5% $Pd_2(dba)_3$, 7.5% TFP, THF, 55 °C; ii) NCS, NaI, AcOH, r.t; iii) H_2N-$(CH_2)_3$-$SiOEt_3$, CH_3CN/CH_2Cl_2 (1:1), r.t.

Scheme 1. Synthesis of BODIPYs **BDP1** and **BDP2**

Synthesis of BDP2. To a solution of 2I-ThioBDP (58.6 mg, 0.11 mmol, 1.0 equiv.) in dry CH_3CN (5 mL) and CH_2Cl_2 (5 mL) was added dropwise (3-aminopropyl)triethoxysilane (0.04 mL, 0.17 mmol, 1.5 equiv) under argon atmosphere at room temperature and the resulting mixture was stirred for 1 h. The solvent was removed in vacuo and the crude product was dissolved in CH_2Cl_2, washed with 10% aqueous HCl solution and water, dried over $MgSO_4$, filtered, and the volatiles were removed in vacuo and the product was purified by flash chromatography on silica gel using hexane/CH_2Cl_2 (5:5) as eluent. The desired product was obtained as a yellow solid (41.4 mg, 0.06 mmol, 53%). M.p. 130.8-131.6 ºC. ^{1}H NMR (700 MHz, $CDCl_3$) δ 7.13 (broad s, 2H, 2CH), 6.93 (t, *J* = 4.2 Hz, 1H , NH), 3.88 (q, *J* = 7.0 Hz, 6H, $3CH_2$), 3.62 (q, *J* = 7.0 Hz, 2H, NCH_2), 2.56 (s, 6H, $2CH_3$), 1.97 (quint, *J* = 7.0 Hz, 2H, CH_2), 1.26 (t, *J* = 7.0 Hz, 9H, $3CH_3$), 0.79 (t, *J* = 7.0 Hz, 2H, $SiCH_2$) ppm. ^{13}C NMR (176 MHz, $CDCl_3$) δ 148.4, 129.7, 124.2 (CH), 121.1, 71.8 (C-I), 58.9 (CH_2), 49.3 (CH_2), 22.1 (CH_2), 18.3 (CH_3), 14.5 (CH_3), 7.9 (CH_2) ppm. FTIR ν 3309, 2922, 2853, 1719, 1583, 1556,

View Article Online
DOI: 10.1039/C7CP01333G

1465, 1369, 1282, 1164, 1080, 960, 794 cm^{-1}. HRMS m/z 691.0203 (calcd for $C_{20}H_{30}BF_2I_2N_3O_3Si$: 691.0207).

2.2.Synthesis of the core-shell nanoparticles

First, 0.1 g of CTAB was dissolved in 50 mL of NH_4OH at 60 ºC. When CTAB was dissolved, 0.8 mL TEOS (0.2 M in EtOH) was added. After 5 h with vigorous stirring at 60 ºC, 0.8 mL of TEOS (1 M in EtOH, 0.8 mmol) and 0.8 mL of an APTMS solution (12% v/v in EtOH, 0.007 mmol) were added and left 24 h more at 60 ºC (Figure 2).

For bioimaging, Rhodamine dyes (10^{-2} to 5.0 $x10^{-5}$ M) were directly added to the synthesis gel. After 24 h, the temperature was decreased to 20 ºC and the mixture was left with vigorous stirring for 12 h more. The NPs were collected by centrifugation of the NP suspension at 12000 rpm at room temperature for 10 min. The collected solid was washed three times in a mixture of miliQ water/EtOH and a fourth time with EtOH only. The surfactant was removed by stirring the NPs with concentrated HCl (0.2 g of HCl in EtOH) for 12 h. The NPs were collected by filtration.

The nanoparticles will be denoted NP (without embedded Rhodamine), NP-Rh6G-x (with x the number of μmole of Rh6G/g of xerogel) or NP-Rh640 depending on the Rhodamine used. The amount of dye embedded into the NP "core" was estimated photometrically, by dissolving the silica matrix with KOH.

2.3. Grafting of photosensitizers on the NP surface through NH_2 groups (NP-RB1 and NP-BDP1)

RB1 (3 x 10^{-2} mmol) was first dissolved in dry THF (20 mL). Then N-hydroxysuccimide (NHS, 0.49 mmol) and N-(3-(dimehylaminopropyl)-N'-ethylcarbodiimide (EDC, 0.46 mmol) was added to activate the carboxylic groups of the PS.[55,31] After 1 hour stirring under argon at RT, dry NP (40 mg) and triethyl amine (TEA, 3.6 x 10^{-2} mol) were added. The reactants were stirred for 3 hours. Next, grafted NPs were washed with THF until the supernatant was completed colorless and collected by filtration (Scheme S1, ESI). However, since BDP1 decomposed under these conditions, an alternative synthesis was performed using as reactant ethyl chloroformate (Acros) and TEA. First the PS (0.027 mmol) was dissolved in dry THF (25 mL) and ethyl chloroformate (1.6 x 10^{-4} mol, 15 μL) and TEA (1.6 x 10^{-4} mol, 22 μL) were added drop by drop. The reaction was carried out under argon at 0 ºC for 30 minutes. Then, the NPs were added and the reaction mixture was stirred at room temperature for 30 minutes. The NPs were washed with THF until the supernatant was completely clear and collected by filtration.

2.4. Grafting of PS on NP surface through OH groups (NP-RB2 and NP-BDP2)

Grafting of RB2 on surface silanols (NP-RB2). First, RB1 (6 x 10^{-3} mmol) was dissolved in dry THF (20 mL) and then NHS (0.14 mmol) and EDC (0.1 mmol) was added. After 1 h stirring under argon, APTMS (2.8 x 10^{-2} mmol) was added to get RB2 within 30 minutes. Immediately the NPs (15 mg) were added and the reaction mixture was stirred for 3 h. The grafted NP-RB2 were washed with THF until the surpernatant was completely colorless and collected by filtration, (Scheme S1, ESI).

2.5. Grafting of BDP2 on surface silanols (NP-BDP2)

BDP2 (5.1 x 10^{-2} mmol) was dissolved in dry THF (20 mL) under argon. Then NPs (28 mg) were added and the reaction mixture was stirred for 3 h. Immediately the NPs were washed with THF until the surpernatant was completely clean and collected by filtration (Scheme S1, ESI). For NPs with dual properties, the synthesis procedures described above were combined (embedding rhodamine in the core and grafting different PS in the shell).

2.6. Characterization

The size, shape and morphology of the silica nanoparticles were characterized by scanning electron microscopy (SEM) and transmission electron microscopy (TEM). SEM images were recorded on a JEOL JSM-6400 and TEM images were produced on a Philips SuperTwin CM200 at 200 kV. The nanoparticle size distribution was analyzed with ImageJ software. Dynamic light scattering (DLS) was used to estimate the NP size in suspension (Malvem Zetasizer Nano ZS with Helium-Neon (λ = 633 nm) laser.

The elements at the sub-surface of the mesoporous silica nanoparticles were analysed by X-Ray photoelectron Spectroscopy (XPS, SPECS equipment). The measurements were carried out by wide scan: energy step 0.1 eV, dwell time 0.1 s, pass energy 30 eV with 90º of electron exit angle. IR-ATR spectra were recorded on a IRAffinity-1S Shimadzu spectrometer in a 4000-400 cm^{-1} range. The silica nanoparticle absorption spectra were recorded on a UV-Vis-NIR spectrophotometer (Cary 7000) with two lamps (halogen lamp for the Vis-IR region and deuterium lamp for the UV region), a double monochromator (Littrow) and double diffraction grating 1200 lines/mm and an integrating sphere (Internal DRA 900).

The total amount of grafted PS was evaluated by two different approaches: 1) by dissolving the silica nanoparticles in tetrabutylammonium fluoride salt (Meth. 1 in Table 1) or 2) by the photometric reading of a previously weighed amount of grafted nanoparticles in suspension, assuming the same molar extinction of the PS in the NP and in solution (Meth. 2 in Table 1). The first method is more accurate, since in the second approach very stable suspensions are required because the aggregation and/or flocculation of the nanoparticles will induce an under-estimation of the absorbance and consequently of the dye concentration. Accordingly the first method was applied to NP-RB1 and NP-RB2 since the BDP chromophores were decomposed in NP-BDP1 and NP-BDP2 after this treatment. Therefore, the BDP loading was estimated

View Article Online
DOI: 10.1039/C7CP01333G

by method 2 for these latter samples since they gave relatively stable suspensions.

The fluorescence and singlet oxygen measurements were recorded with an Edinburgh spectrofluorimeter (FLSP920 model) equipped with a 450 W xenon flash lamp. The fluorescence spectra were corrected for the wavelength dependence of the detector sensitivity. Radiative decay curves were recorded with time-correlated single-photon counting (Edinburgh Instruments, model FL920) using a microchannel plate detector (Hamamatsu C4878) with picosecond time resolution. The singlet oxygen quantum yields were determined by direct measurement of the luminescence at 1270 nm with a NIR detector integrated in the spectrofluorimeter (InGaAs detector, Hamamatsu G8605-23) using as reference RB1 in ACN and the already described 8-methylthio-2,6-diiodo BODIPY (2I-Thio-BDP) in $CHCl_3$.[29]

Conclusions

Spherical core-shell silica NPs with an external surface functionalized by amino groups and with an average size around 50 nm have been synthesized. The external surface was grafted with commercial (Rose Bengal) or novel lab-made PSs (BODIPY). Accurate determinations showed that good singlet oxygen quantum yields (Φ_Δ ~ 0.35-0.40) were obtained in acetonitrile and chloroform with novel halogenated BODIPY grafted to the external shell of silica. Such quantum yields are globally much higher than those of similar NPs using grafted RB as PS (Φ_Δ ~ 0.10-0.27). These results were related to the agglomeration of NPs, which depends both on the type of photosensitizer and on the grafting method. We thus confirm that the use of BODIPYs as photosensitizers may offer a good alternative to commercial RB. Advantages are a lower tendency to agglomerate NPs, their good quantum yield of singlet oxygen production, together with their easy functionalization in order to tune their photophysical properties and the possibility of grafting on various substrates.

Encapsulation of fluorescent rhodamines in the core at an optimal concentration led to good fluorescence quantum yields ($\Phi_{fl} \geq 0.3$), which allowed their tracking by fluorescence microscopy. Finally, combining complementary actions under the same excitation light, namely a fluorescent rhodamine in the core and a sensitizer with an overlapping absorption band in the shell, NPs with dual functionality were obtained (Φ_{fl} 0.10-0.20, Φ_Δ 0.16-0.25). The results also show that efficient FRET is possible in such NPs when combining a fluorescent dye in the core and a PS grafted in the shell, due to the very close proximity of the dyes. This FRET process is strongly detrimental to singlet oxygen production.

Fine tuning of singlet oxygen production, fluorescence emission or alternatively of FRET process efficiency is thus necessary and possible by proper choice of the dyes, of their concentration inside and on the NPs, and of the grafting method.

This study emphasizes the importance of the NP suspension stability to accurately address the determination of their photophysical properties. The next step of this work is improving the stability of the NP suspensions in water for *in vitro* phototoxicity experiments.

Acknowledgements

The authors thank the Spanish Ministry of Economy and Competitiveness, MINECO, (MAT 2014-51937-C3-3, MAT 2014-51937-C3-2 and MAT2015-68837-REDT) and Basque Government (IT912-16) for funding this research. VMM acknowledge Ministerio de Economía y Competitividad MINECO for 'Ramón y Cajal' contract (RYC-2011-09505). NEE acknowledges Universidad del País Vasco (UPV-EHU) for a predoctoral contract and Université de Pau et Pays de l'Adour (UPPA) together with UPV-EHU for a co-advised doctoral grant. E. P.-C. wishes to thank CONACyT (Grants 129572 and 123732).

Notes and references

[1] A. A. Ghogare and A. Greer, *Chem. Rev.*, 2016, **116**, 9994–10034.
[2] K. Zhang, Z. Vobecka, K. Tauer, M. Antonietti and F. Vilela, *Chem. Commun.*, 2013, **49**, 11158–11160.
[3] J. Shen, R. Steinbach, J. M. Tobin, M. Mouro Nakata, M. Bower, M. R. S. McCoustra, H. Bridle, V. Arrighi and F. Vilela, *Appl. Catal. B Environ.*, 2016, **193**, 226–233.
[4] S. G. Awuah and Y. You, *RSC Adv.*, 2012, **2**, 11169.
[5] A. Kamkaew, S. H. Lim, H. B. Lee, L. V. Kiew, L. Y. Chung and K. Burgess, *Chem. Soc. Rev.*, 2013, **42**, 77–88.
[6] H. Abrahamse and M. R. Hamblin, *Biochem. J.*, 2016, **473**, 347–364.
[7] S. Lacombe and T. Pigot, *Catal. Sci. Technol.*, 2016, **6**, 1571–1592.
[8] S. S. Lucky, K. C. Soo and Y. Zhang, *Chem. Rev.*, 2015, **115**, 1990–2042.
[9] K. K. Cotí, M. E. Belowich, M. Liong, M. W. Ambrogio, Y. a Lau, H. a Khatib, J. I. Zink, N. M. Khashab and J. F. Stoddart, *Nanoscale*, 2009, **1**, 16–39.
[10] Y. Wang, Q. Zhao, N. Han, L. Bai, J. Li, J. Liu, E. Che, L. Hu, Q. Zhang, T. Jiang and S. Wang, *Nanomedicine Nanotechnol. Biol. Med.*, 2015, **11**, 313–327.
[11] V. Mamaeva, C. Sahlgren and M. Lindén, *Adv. Drug Deliv. Rev.*, 2013, **65**, 689–702.
[12] P. Couleaud, V. Morosini, C. Frochot, S. Richeter, L. Raehm and J.-O. Durand, *Nanoscale*, 2010, **2**, 1083–1095.
[13] L. Zhou, W. Wang, S. H. Wei, Y. Y. Feng, J. H. Zhou, J. H. Liu and J. Shen, *J. Porous Mater.*, 2010, **18**, 517–522.
[14] H. Liu, Y. Yang, A. Wang, M. Han, W. Cui and J. Li, *Adv. Funct. Mater.*, 2016, **26**, 2561–2570.
[15] I. Roy, T. Y. Ohulchanskyy, H. E. Pudavar, E. J. Bergey, A. R. Oseroff, J. Morgan, T. J. Dougherty and P. N. Prasad, *J. Am. Chem. Soc.*, 2003, **125**, 7860–7865.
[16] T. Y. Ohulchanskyy, I. Roy, L. N. Goswami, Y. Chen, E. J. Bergey, R. K. Pandey, A. R. Oseroff and P. N. Prasad, *Nano Lett.*, 2007, **7**, 2835–2842.
[17] Y.-S. Lin, C.-P. Tsai, H.-Y. Huang, C.-T. Kuo, Y. Hung, D.-M. Huang, Y.-C. Chen and C.-Y. Mou, *Chem. Mater.*, 2005, **17**, 4570–4573.
[18] E. Rampazzo, S. Bonacchi, D. Genovese, R. Juris, M. Sgarzi, M. Montalti, L. Prodi, N. Zaccheroni, G. Tomaselli, S. Gentile, C. Satriano and E. Rizzarelli, *Chem. - Eur. J.*, 2011, **17**, 13429–13432.
[19] E. Rampazzo, S. Bonacchi, D. Genovese, R. Juris, M. Montalti, V. Paterlini, N. Zaccheroni, C. Dumas-Verdes, G.

View Article Online
DOI: 10.1039/C7CP01333G

Clavier, R. Méallet-Renault and L. Prodi, *J. Phys. Chem. C*, 2014, **118**, 9261–9267.
[20] M. Galli, E. Moschini, M. V. Dozzi, P. Arosio, M. Panigati, L. D'Alfonso, P. Mantecca, A. Lascialfari, G. D'Alfonso and D. Maggioni, *RSC Adv.*, 2016, **6**, 38521–38532.
[21] K. K. Ng and G. Zheng, *Chem. Rev.*, 2015, **115**, 11012–11042.
[22] B. M. Estevão, I. Miletto, L. Marchese and E. Gianotti, *Phys. Chem. Chem. Phys.*, 2016, **18**, 9042–9052.
[23] T. Zhang, H. Lin, L. Cui, N. An, R. Tong, Y. Chen, C. Yang, X. Li, J. Liu and F. Qu, *Eur. J. Inorg. Chem.*, 2016, **2016**, 1206–1213.
[24] H. Wang, R. Han, L. Yang, J. Shi, Z. Liu, Y. Hu, Y. Wang, S. Liu and Y. Gan, *ACS Appl. Mater. Interfaces*, 2016, **8**, 4416–4423.
[25] M. A. Malvindi, V. Brunetti, G. Vecchio, A. Galeone, R. Cingolani and P. P. Pompa, *Nanoscale*, 2012, **4**, 486.
[26] J. E. Lee, N. Lee, T. Kim, J. Kim and T. Hyeon, *Acc. Chem. Res.*, 2011, **44**, 893–902.
[27] H. Ow, D. R. Larson, M. Srivastava, B. a. Baird, W. W. Webb and U. Wiesnert, *Nano Lett.*, 2005, **5**, 113–117.
[28] S. Luo, E. Zhang, Y. Su, T. Cheng and C. Shi, *Biomaterials*, 2011, **32**, 7127–7138.
[29] M. C. DeRosa and R. J. Crutchley, *Coord. Chem. Rev.*, 2002, **233–234**, 351–371.
[30] J. Paczkowski and D. C. Neckers, *J. Photochem.*, 1986, **35**, 283–287.
[31] F. Ronzani, N. Costarramone, S. Blanc, A. K. Benabbou, M. Le Bechec, T. Pigot, M. Oelgemöller and S. Lacombe, *J. Catal.*, **303**, 164–174.
[32] T. Yogo, Y. Urano, Y. Ishitsuka, F. Maniwa and T. Nagano, *J. Am. Chem. Soc.*, 2005, **127**, 12162–12163.
[33] G. Ulrich, R. Ziessel and A. Harriman, *Angew. Chem. Int. Ed Engl.*, 2008, **47**, 1184–201.
[34] J. Zhao, W. Wu, J. Sun and S. Guo, *Chem. Soc. Rev.*, 2013, **42**, 5323–51.
[35] N. Epelde-Elezcano, V. Martínez-Martínez, E. Peña-Cabrera, C. F. A. Gómez-Durán, I. L. Arbeloa and S. Lacombe, *RSC Adv*, 2016, **6**, 41991–41998.
[36] B. Kim, B. Sui, X. Yue, S. Tang, M. G. Tichy and K. D. Belfield, *Eur. J. Org. Chem.*, 2017, **2017**, 25–28.
[37] A. J. Sánchez-Arroyo, E. Palao, A. R. Agarrabeitia, M. J. Ortiz and D. García-Fresnadillo, *Phys. Chem. Chem. Phys.*, 2016, **19**, 69–72.
[38] Q. Zhang, Y. Cai, X.-J. Wang, J.-L. Xu, Z. Ye, S. Wang, P. H. Seeberger and J. Yin, *ACS Appl. Mater. Interfaces*, 2016, **8**, 33405–33411.
[39] L. Huang, Z. Li, Y. Zhao, Y. Zhang, S. Wu, J. Zhao and G. Han, *J. Am. Chem. Soc.*, 2016, **138**, 14586–14591.
[40] V. Valtchev and L. Tosheva, *Chem. Rev.*, 2013, **113**, 6734–60.
[41] F. Hoffmann, M. Cornelius, J. Morell and M. Fröba, *Angew. Chem. Int. Ed.*, 2006, **45**, 3216–3251.
[42] T. V. Goud, A. Tutar and J. F. Biellmann, *Tetrahedron*, 2006, **62**, 5084–5091.
[43] S. Kolemen, O. A. Bozdemir, Y. Cakmak, G. Barin, S. Erten-Ela, M. Marszalek, J.-H. Yum, S. M. Zakeeruddin, M. K. Nazeeruddin, M. Grätzel and E. U. Akkaya, *Chem. Sci.*, 2011, **2**, 949–954.
[44] B. Martins Estevão, F. Cucinotta, N. Hioka, M. Cossi, M. Argeri, G. Paul, L. Marchese and E. Gianotti, *Phys Chem Chem Phys*, 2015, **17**, 26804–26812.
[45] D. Magde, G. E. Rojas ' and P. G. Seybold2, *Photochem. Photobiol.*, 1999, **70**, 737–744.
[46] S. Guo, H. Zhang, L. Huang, Z. Guo, G. Xiong and J. Zhao, *Chem. Commun.*, 2013, **49**, 8689–8691.
[47] A. Uppal, B. Jain, P. K. Gupta and K. Das, *Photochem. Photobiol.*, 2011, **87**, 1146–1151.
[48] E. Gianotti, B. MartinsEstevão, F. Cucinotta, N. Hioka, M. Rizzi, F. Renò and L. Marchese, *Chem. - Eur. J.*, 2014, 10921–10925.
[49] P.-A. Cazade, P. Bordat, S. Blanc, I. Baraille and R. Brown, *Langmuir*, 2008, **24**, 2252–2257.
[50] Z. Wang, X. Hong, S. Zong, C. Tang, Y. Cui and Q. Zheng, *Sci. Rep.*, 2015, **5**, 12602.
[51] C. G. Martínez, A. Neuner, C. Martí, S. Nonell, A. M. Braun and E. Oliveros, *Helv. Chim. Acta*, 2003, **86**, 384–397.
[52] A. Sève, P. Couleaud, F. Lux, O. Tillement, P. Arnoux, J.-C. André and C. Frochot, *Photochem. Photobiol. Sci.*, 2012, **11**, 803.
[53] Joseph R. Lakowicz, *Principles of Fluorescence Spectroscopy*, Springer, Baltimore, USA, Third Edit., 1999.
[54] R. Zhang, C. Wu, L. Tong, B. Tang and Q.-H. Xu, *Langmuir*, 2009, **25**, 10153–10158.
[55] S.-H. Cheng, C.-H. Lee, C.-S. Yang, F.-G. Tseng, C.-Y. Mou and L.-W. Lo, *J. Mater. Chem.*, 2009, **19**, 1252–1257.